DOI: 10.1002/ejic.200601084

CuO/ZnO Nanoparticles in a Matrix of Amorphous Silica as High-Surface Precursors for Methanol Synthesis

Bernd Rohe,[a] Rainer Weiss,[b] Sascha Vukojević,[c] Christian Baltes,[c] Martin Muhler,[d] Michael Tausch,[e] and Matthias Epple*[b]

Keywords: Heterogeneous catalysis / Copper / Zinc oxide / Silica / Nanoparticles / Surface coating

An intimate mixture of CuO/ZnO nanocrystals was prepared by an easy sol-gel synthesis (precipitation in methanol by hydroxide in the presence of a silane). The organic substituents of the silane were almost completely removed by a subsequent photochemical oxidation. The resulting amorphous SiO_2 prevented the growth of the catalytically active particles to larger crystals. The coating layer of silica can easily be penetrated by gaseous reactants, as shown by the high specific surface area of about 110–130 $m^2 g^{-1}$ (probably due to both silica and nanocrystalline CuO/ZnO) and the good catalytic activity in methanol synthesis from $CO/CO_2/H_2$ synthesis gas (7 to 37 %, compared to an industrial standard methanol catalyst). The ratio of CuO to ZnO can be easily varied by the used preparation method.

Introduction

Cu/ZnO is a widely used model catalyst system for investigations in heterogeneous catalysis.[1] In most cases, the methanol synthesis and the steam reforming reaction are studied. The industrial catalyst is based on Cu/ZnO/Al_2O_3,[1,2] but often Cu/ZnO is examined as simplified binary model system.[3–15] Although copper is the more important catalytically active component,[16,17] pure ZnO is itself active in methanol synthesis[18–20] The most common preparation methods for the catalyst precursor CuO/ZnO are based on the co-precipitation of carbonates or oxalates, followed by thermolysis to the corresponding oxides.[6,8,11,14,21–23] We have recently shown that active catalysts can also be prepared by thermolysis of bimetallic coordination compounds,[24] xerogels and aerogels,[25] and tartrate mixed crystals.[26] Copper nanoparticles in liquid dispersion were recently shown to be active as methanol catalysts,[27] as well as metal-loaded mesoporous silicates[28] and metal-oxide frameworks (MOFs).[29]

Here we report on the preparation, characterization and catalytic activity of ZnO and CuO/ZnO nanocomposites which were obtained by a combination of sol-gel synthesis and photochemical oxidation which was applied earlier to prepare nanoscale ZnO.[30] By precipitating the oxides in the presence of a silane in alcohol, a highly dispersed mixture of the oxides with a high specific surface area[31] is obtained because the silane prevents the growth and agglomeration of the oxide crystals.[32] Subsequently, the organic substituents of the silane are photochemically oxidized and almost completely removed.[30] The ratio of copper to zinc can be easily varied by this method, opening a way to nanocrystalline systems of CuO/ZnO in amorphous silica with a high overall specific surface area. Copper oxide can then be reduced to Cu, resulting in Cu/ZnO/SiO_2, i.e. the active methanol catalyst, preserving a high specific surface area which is advantageous for a high catalytic activity. This approach to co-precipitate the nanoparticles with a porous inorganic matrix is different from the often applied approach to fill an already existing porous template.

[a] Sachtleben Chemie GmbH,
Dr.-Rudolf-Sachtleben-Str. 4, 47198 Duisburg, Germany
[b] Inorganic Chemistry, University of Duisburg-Essen,
Universitätsstrasse 5–7, 45117 Essen, Germany
Fax: +49-201-183-2621
[c] Max-Planck-Institute for Coal Research,
Kaiser-Wilhelm-Platz 1, 45470 Mülheim an der Ruhr, Germany
[d] Industrial Chemistry, Ruhr University of Bochum,
Universitaetsstrasse 150, 44801 Bochum, Germany
[e] University of Wuppertal,
Gaussstr. 20, 42119 Wuppertal, Germany

Result and Discussion

Four samples with different ratios of CuO/ZnO (**A**: 0.76 wt.-% Cu; **B**: 4.37 wt.-% Cu; **C**: 15.6 wt.-% Cu; **D**: 34.4 wt.-% Cu) were prepared by a combination of sol-gel synthesis and photochemical oxidation and compared to a sample of pure ZnO (**Z**), prepared by the same method.[30] The coating with silane prevented crystal growth and agglomeration of the primary oxides. The subsequent photochemical treatment almost completely destroyed the organic fragments of the silane and led to the formation of X-ray amorphous silica ("SiO_2").

Scanning electron microscopy (SEM) showed an agglomerated material with particle sizes of a few hundred nano-

metres (Figure 1). The "coating layer" probably results from amorphous silica which remains after the photochemical oxidation. The high specific surface area from BET experiments (Table 1) indicates a high internal porosity that we tentatively attribute to the silica. X-ray powder diffraction shows broad diffraction peaks for ZnO and CuO, confirming the nanocrystallinity of the primary particles (Figure 2). A semi-quantitative determination of the crystallite size for ZnO by the Scherrer equation[33] results in 6–7 nm. It was not possible to determine the size of the CuO particles due to peak overlap, but a visual examination of the peak in Figure 2 suggests a crystallite size of the same order. Temperature-programmed reduction (TPR) gave the amount of CuO (Figure 3), followed by the quantitative determination of the specific copper surface area with reactive frontal chromatography (RFC). All analytical results are comprised in Table 1. It should be noted that the content of zinc is in all cases lower than expected from the synthesis (Table 1). This means that copper preferentially precipitates during the synthesis.

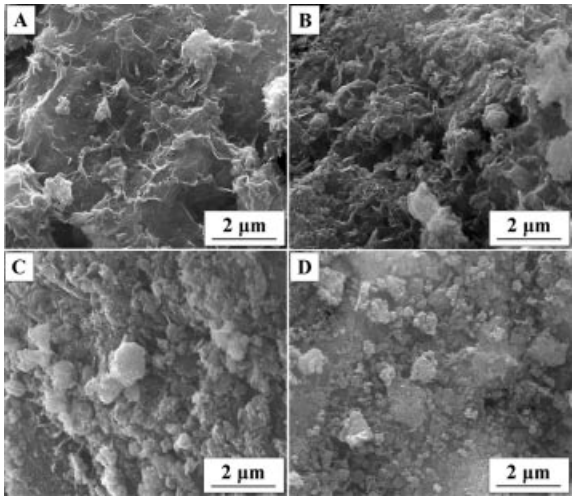

Figure 1. Scanning electron micrographs of the CuO/ZnO samples **A** to **D** (see Table 1). The samples consist of agglomerated particles with sizes of a few hundred nanometers (**A**: 0.76 wt.-% Cu; **B**: 4.37 wt.-% Cu; **C**: 15.6 wt.-% Cu; **D**: 34.4 wt.-% Cu). CuO and ZnO cannot be distinguished, i.e. they form an intimate mixture, together with X-ray amorphous SiO_2.

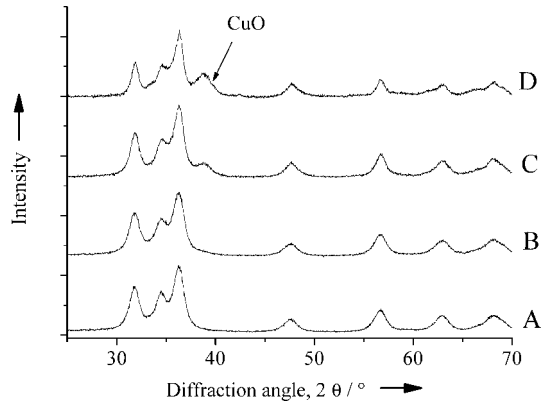

Figure 2. X-ray powder diffraction patterns of samples **A**, **B**, **C** and **D**. All reflections of the samples **A** and **B** belong to ZnO (zincite), except for the reflection at 38.9 °2Θ which belongs to CuO (tenorite). All patterns show strong peak broadening due to the small size of the primary nanoparticles (**A**: 0.76 wt.-% Cu; **B**: 4.37 wt.-% Cu; **C**: 15.6 wt.-% Cu; **D**: 34.4 wt.-% Cu).

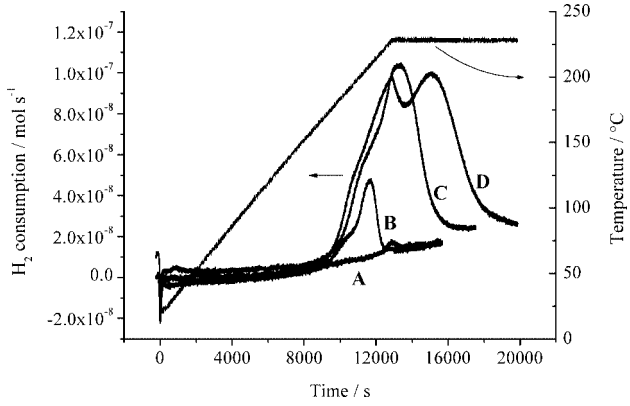

Figure 3. Reduction profiles of CuO to Cu obtained by heating under diluted hydrogen (TPR: temperature-programmed reduction; **A**: 0.76 wt.-% Cu; **B**: 4.37 wt.-% Cu; **C**: 15.6 wt.-% Cu; **D**: 34.4 wt.-% Cu).

The total specific surface area was determined by BET after drying for 2 h at 110 °C under air (Table 1). The BET surface areas were very high (higher than those of CuO/ZnO from co-precipitated carbonate precursors which are typically 40 $m^2 g^{-1}$ or less[31]). In addition, they are almost

Table 1. Chemical and morphological parameters and catalytic activity of all samples.

Sample	wt.-%[a] Zn	wt.-%[a] Cu	wt.-% Cu (by TPR)	wt.-%[b] C	wt.-%[b] H	wt.-%[b] SiO_2	ZnO crystallite size[d] / nm	Specific surface area[a,e] / $m^2 g^{-1}$	Specific Cu surface[a–f] area / $m^2 g^{-1}$	Catalytic activity (%)[g]
Z (pure ZnO)	67.0	0.0	–	2.6	0.8	16.6	6	127.8	0.0	–
A (CuO/ZnO)	66.4	0.76	0.3	2.2	0.7	13.5	6	110.0	0.1	7
B (CuO/ZnO)	61.2	4.37	3.7	2.6	0.5	15.3	6	134.8	0.3	16
C (CuO/ZnO)	53.3	15.6	13.6	2.9	0.6	10.6	7	132.0	0.3	35
D (CuO/ZnO)	35.7	34.4	26.8	3.2	0.6	8.7	7	113.3	5.5	37

[a] By ICP. [b] By combustion elemental analysis. [c] The contents of zinc and copper were used to compute the amount of ZnO and CuO in the sample (stoichiometric factors 1.245 and 1.252, respectively). The sum of ZnO, ZnO, C and H was computed, and the difference to 100% was tentatively ascribed to SiO_2. [d] By application of the Scherrer equation;[33] the full-width at half maximum (FWHM) was typically 1.2–1.6° 2Θ for the (102), (110), and (103) peaks of ZnO with no differences among these peaks. [e] By BET. [f] By reactive frontal chromatography (RFC). [g] Compared to the activity of an ICI reference methanol catalyst, consisting of 64 wt.-% CuO, 24 wt.-% ZnO and 10 wt.-% Al_2O_3 (data from the manufacturer).

independent from the composition of the samples, suggesting that silica is mostly responsible for this high surface area. We conclude that the nature of the metal cation does not play a significant role for the micromorphology of the precatalyst, and we also conclude that most of the surface must be ascribed to internal pores, given the fact that the samples appear agglomerated and not nanoparticulate in SEM. The amorphous silicon dioxide which is left after photooxidation[30,32] is probably responsible for this effect, preventing the fusion of the oxide nanoparticles by formation of a porous coating layer. Note that the UV-photooxidation is not complete, as indicated by the residual content of carbon and hydrogen (Table 1) and also by weak characteristic C–H vibrations in IR spectroscopy (data not shown). In total, about 10–15 wt.-% of silica and carbon-containing residues together are present in the samples (see Table 1), both being X-ray amorphous (Figure 2).

This coating effect may explain the comparatively small specific copper surface area obtained by reactive frontal chromatography (RFC). Except for a very high content of copper, the copper surface area is small compared to the BET surface areas, unlike oxide mixtures from carbonate precursors.[31] We assume sintering of the copper particles due to the high reduction temperature (>200 °C) which caused a small specific surface area. Nevertheless, the catalytic activity of the samples is much higher than it would have been predicted from this small specific copper surface area.[12] The catalytic activity was compared to a ternary $CuO/ZnO/Al_2O_3$ benchmark catalyst (ICI Katalco 51-8) whose activity was set to 100%. This proves that the silica-embedded copper and zinc oxide particles are still well accessible by the synthesis gas. We speculate that the silica layer itself has a high internal pore surface which can be penetrated by the gaseous molecules, so it also serves as a kind of membrane on the catalytically active particles (ZnO and Cu).

We explain the mismatch between the low specific copper surface area and the good catalytic activity as follows: the specific copper surface area after TPR does not correspond to the copper surface area which is present in the active catalyst because of different reduction conditions. In TPR which is followed by RFC, CuO is reduced with diluted hydrogen (4.1% H_2 in Ar) at atmospheric pressure at 223 °C. Figure 3 shows that the reduction temperature is comparatively high, i.e. the copper oxide is not easily reduced (possibly not even fully, but mostly; see Table 1). In the catalytic test, the catalyst is reduced by a prescribed procedure for the commercial catalyst involving several steps, e.g. heating to 170 °C in 5% H_2/N_2, keeping it at that temperature for a certain period of time, then increasing the temperature and the concentration of H_2 and finally reaching 245 °C in pure H_2 under 25 bar pressure. Subsequently and prior to the measurement of the catalytic activity, the catalysts are equilibrated at the final operating pressure and gas composition mixture ($H_2/CO/CO_2$). Therefore, it is likely that there is a difference between the copper surface area measured by RFC and the copper surface area of the materials during catalytic testing (it is well known that dynamic effects are controlling the size and shape of the Cu crystals during reduction[4,7]). The fact that the content of copper found by TPR is about 20% smaller than the content of copper by elemental analysis may indicate an incomplete reduction due to a surface layer of impenetrable silica. However, this also indicates that most of the copper (about 80%) was reduced. The small specific copper surface area may be due to sintering of the crystals under the TPR conditions which does not occur upon reduction under higher pressure in the parallel reactor.

Conclusions

$CuO/ZnO/SiO_2$ composites with high specific surface area and good catalytic activity in heterogeneous methanol synthesis can be prepared by a combination of sol-gel chemistry and photochemistry. The ratio of copper to zinc can be easily varied in the precipitation process. The primary nanoparticles of ZnO and CuO are covered by silica, but still accessible for gases as demonstrated by the high BET surface area (indicating pores in the silica) and the good catalytic activity. The catalytic activity increases with the content of copper oxide in the precatalyst. The X-ray amorphous silica prevents the fusion of the catalytically active CuO/ZnO nanoparticles and also serves as a membrane which can be penetrated by the gaseous reactants (CO, CO_2, H_2, CH_3OH).

Experimental Section

Sol-Gel Synthesis and Photochemical Oxidation: In the first step, silane-coated CuO/ZnO was synthesized according to refs.[30,32]. 11.12 g (45 mmol) (3-methacryloxypropyl)trimethoxysilane was added to 333 g methanol at 55 °C in a 1-L round-bottomed flask. At 60 °C, zinc acetate dihydrate and copper acetate monohydrate were added (Table 2) and a solution of 50.3 g (0.89 mol) potassium hydroxide in 167 g methanol was added dropwise. The precipitate was filtered off and washed four times with methanol. After centrifugation of the gelatineous precipitate, the product was dried at 130 °C. In the second step, 1.5 g of the synthesized silane-coated CuO/ZnO were dispersed in 450 mL water and transferred into a water-cooled UV-lamp reactor. The suspension was irradiated with a 125-W mercury high-pressure lamp (HPK 125 W, Philips) for 60 min whilst stirring to destroy the organic parts of the silane while bubbling air through the dispersion. The material was then centrifuged (10 min, 2000 rpm) and dried at 150 °C for 24 h.

Table 2. Preparation conditions of all samples.

Sample	*n*(zinc acetate dihydrate) /(mmol)	*n*(copper(II) acetate monohydrate) /(mmol)
Z	448	–
A	448	5
B	448	23
C	405	45
D	336	123

Solid-State Characterization Methods: BET measurements were conducted with a Micromeritics instrument Flow Sorb II 2300. Ele-

mental analysis of copper and zinc were carried out with an inductively coupled plasma-optical emission spectrometer (ICP-OES) Varian VISTA MPX with a radial plasma. X-ray powder diffraction (XRD) was performed on a Siemens D 500 instrument with Cu-K_α radiation. Scanning electron microscopy was performed with a FEI ESEM Quanta 400 FEG instrument on gold-sputtered samples.

Catalytic Performance: Measurements were performed in a high-throughput 49-parallel channel reactor.[11] The samples (100 mg diluted with 200 mg quartz per well) were placed in a sample holder consisting of a stainless steel cartridge closed at the bottom by a stainless-steel sinter metal frit. Prior to the catalytic measurements the catalysts were reduced with a H_2/N_2 mixture at 518 K following the prescribed procedure for the commercial benchmark catalyst ICI Katalco 51-8 (see above). Before measuring the catalytic activity, all samples were equilibrated for 3 h (reaction pressure 4.5 MPa, reaction temperature 518 K, analytic flow 20 mL min^{-1}). The reaction gas consisted of 70% H_2, 24% CO, and 6% CO_2. A double GC system (HP GC 6890) equipped with a methanizer FID was used for online gas analysis. Oxo-product separation (H_3COH, $HCOOCH_3$, $H_3CCOOCH_3$, H_3CCH_2OH) was carried out on a SuppelcoWAX 0.53 mm column and CO, CO_2 and CH_4 were separated on a Carboxen 1006 column. Methanol productivities for all measured samples were compared to the productivity of the industrial benchmark catalyst ICI Katalco 51-8 (P_{ICI} = 40 mol MeOH/(kg_{cat} h) at 518 K and 4.5 MPa).

Temperature-Programmed Reduction (TPR) and Reactive Frontal Chromatography (RFC): The set-up used for TPR and N_2O RFC consisted of a gas supply unit, a specially designed reactor and furnace, and a gas analysis section. The gas supply unit was equipped with mass flow controllers and included gas lines for pure Ar, a 4.2% H_2/Ar gas mixture, and a 1.0% N_2O/Ar gas mixture. The reactor was made of two concentric quartz tubes of an optimized geometry with respect to back-mixing of gas and the axial temperature profile. The design of the reactor and the furnace followed the work of Monti and Baiker.[34] The temperature of the furnace was controlled by a programmable PID controller (Eurotherm 2416). The gas analysis section included a cooling trap (filled with isopropyl alcohol and dry ice) for water removal, a thermal conductivity detector (Hydros) to monitor the uptake of H_2, and an dispersive IR detector (Uras) to monitor the uptake of N_2O. The set-up was operated by a personal computer via a program based on the software package LabView.

The TPR experiments were carried out to determine the specific Cu content of samples and to reduce samples prior to N_2O RFC. A 100 mg sample was heated from 303 K to 513 K (furnace temperature; sample temperature 500 K) with a heating rate of 2 K min^{-1} and the final temperature was held for 1 h. The inlet concentration of H_2 was fixed to 4.2% and the total flow rate of the H_2/Ar gas mixture was set to 84 mL min^{-1}. The low values of the heating rate, the final temperature, and the inlet concentration of H_2 were chosen to minimize sintering of the copper particles due to heat released by the reduction process or too high temperature.

The determination of the specific Cu surface area by N_2O RFC was carried out consecutively to the TPR experiment. After cooling to room temperature in the flowing H_2/Ar gas mixture, the reactor was flushed for 15 min with pure Ar (50 mL min^{-1}). After bypassing the reactor and the cooling trap the Uras IR detector was calibrated, first in pure Ar and then in a 1.0% N_2O/Ar gas mixture (10 mL min^{-1}). When the calibration was finished the reactor was set on-line and the uptake of N_2O from the N_2O/Ar gas mixture (10 mL min^{-1}) was measured. The measurement was finished when no further uptake of N_2O was detectable. This method is based on the decomposition of N_2O on exposed Cu atoms accompanied by the formation of adsorbed atomic oxygen O_{ads} and gas-phase N_2. For calculation of the exposed Cu surface area an average surface atom density of 1.47×10^{19} Cu atoms m^{-2} was used. The specific Cu surface area was obtained by dividing the exposed Cu surface area by the initial sample mass [35].

All gas volumes correspond to standard conditions at 0 °C and 1013 mbar.

Acknowledgments

This work was supported by the Deutsche Forschungsgemeinschaft (DFG) within the scope of the Collaborative Research Center SFB 558: Metal-substrate interactions in heterogeneous catalysis. We also acknowledge the support of the experimental section of Grillo-Werke AG, Duisburg. We are grateful to Prof. F. Schüth, Mülheim/Ruhr, for helpful discussions.

[1] J. M. Thomas, W. J. Thomas, *Principles and practice of heterogeneous catalysis*, VCH, Weinheim, **1996**.
[2] J. R. Jensen, T. Johannessen, S. Wedel, H. Livbjerg, *J. Catal.* **2003**, *218*, 67–77.
[3] C. V. Ovesen, B. S. Clausen, J. Schiotz, P. Stoltze, H. Topsøe, J. K. Nørskov, *J. Catal.* **1997**, *168*, 133–142.
[4] J. D. Grunwaldt, A. M. Molenbroek, N. Y. Topsoe, H. Topsoe, B. S. Clausen, *J. Catal.* **2000**, *194*, 452–460.
[5] S. A. French, A. A. Sokol, S. T. Bromley, C. R. A. Catlow, S. C. Rogers, F. King, P. Sherwood, *Angew. Chem.* **2001**, *113*, 4569–4572; *Angew. Chem. Int. Ed.* **2001**, *40*, 4437–4440.
[6] M. M. Günter, T. Ressler, B. Bems, C. Büscher, T. Genger, O. Hinrichsen, M. Muhler, R. Schlögl, *Catal. Lett.* **2001**, *71*, 37–44.
[7] P. L. Hansen, J. B. Wagner, S. Helveg, J. R. Rostrup-Nielsen, B. S. Clausen, H. Topsoe, *Science* **2002**, *295*, 2053–2055.
[8] B. Bems, M. Schur, A. Dassenoy, H. Junkes, D. Herein, R. Schlögl, *Chem. Eur. J.* **2003**, *9*, 2039–2052.
[9] M. C. Carroll, B. Skrotzki, M. Kurtz, M. Muhler, G. Eggeler, *Scripta Mater.* **2003**, *49*, 527–532.
[10] S. A. French, A. A. Sokol, S. T. Bromley, C. R. A. Catlow, P. Sherwood, *Top. Catal.* **2003**, *24*, 161–172.
[11] C. Kiener, M. Kurtz, H. Wilmer, C. Hoffmann, H. W. Schmidt, J. D. Grunwaldt, M. Muhler, F. Schüth, *J. Catal.* **2003**, *216*, 110–119.
[12] M. Kurtz, H. Wilmer, T. Genger, O. Hinrichsen, M. Muhler, *Catal. Lett.* **2003**, *86*, 77–80.
[13] M. Schur, B. Bems, A. Dassenoy, I. Kassatkine, J. Urban, H. Wilmes, O. Hinrichsen, M. Muhler, R. Schlögl, *Angew. Chem.* **2003**, *115*, 3945–3947; *Angew. Chem. Int. Ed.* **2003**, *42*, 3815–3817.
[14] B. L. Kniep, T. Ressler, A. Rabis, F. Girgsdies, M. Baenitz, F. Steglich, R. Schlögl, *Angew. Chem.* **2004**, *116*, 114–117; *Angew. Chem. Int. Ed.* **2004**, *43*, 112–115.
[15] T. Ressler, B. L. Kniep, I. Kasatkin, R. Schlögl, *Angew. Chem.* **2005**, *117*, 4782–4785; *Angew. Chem. Int. Ed.* **2005**, *44*, 4704–4707.
[16] R. B. Rasmussen, P. M. Holmblad, T. Askgaard, C. V. Ovesen, P. Stoltze, J. K. Nørskov, I. Chorkendorff, *Catal. Lett.* **1994**, *26*, 373–381.
[17] J. Yoshihara, C. T. Campbell, *J. Catal.* **1996**, *161*, 776–782.
[18] H. Wilmer, M. Kurtz, K. Klementiev, O. Tkachenko, W. Grünert, O. Hinrichsen, A. Birkner, S. Rabe, K. Merz, M. Driess, C. Wöll, M. Muhler, *Phys. Chem. Chem. Phys.* **2003**, *5*, 4736–4742.
[19] M. Kurtz, J. Strunk, O. Hinrichsen, M. Muhler, K. Fink, B. Meyer, C. Wöll, *Angew. Chem.* **2005**, *117*, 2850–2854; *Angew. Chem. Int. Ed.* **2005**, *44*, 2790–2794.

[20] S. Polarz, J. Strunk, V. Ischenko, M. W. E. van den Berg, O. Hinrichsen, M. Muhler, M. Driess, *Angew. Chem.* **2006**, *118*, 3031–3035; *Angew. Chem. Int. Ed.* **2006**, *45*, 2965–2969.
[21] C. Chauvin, J. Jaussey, J. C. Lavalley, H. Idriss, J. P. Hidermann, A. Kiennemann, P. Chaumette, P. Coutry, *J. Catal.* **1990**, *121*, 56–69.
[22] G. J. Hutchings, J. C. Vedrine, in *Basic principles in applied catalysis, vol. 75* (Ed.: M. Baerns), Springer, New York, **2004**, pp. 217–258.
[23] M. Saito, K. Murata, *Catal. Surveys from Asia* **2004**, *8*, 285–294.
[24] R. Weiss, Y. Guo, S. Vukojevic, L. Khodeir, R. Boese, F. Schüth, M. Muhler, M. Epple, *Eur. J. Inorg. Chem.* **2006**, 1796–1802.
[25] Y. Guo, W. Meyer-Zaika, M. Muhler, S. Vukojevic, M. Epple, *Eur. J. Inorg. Chem.* **2006**, 4774–4781.
[26] R. Weiss, S. Vukojevic, C. Baltes, R. Naumann d'Alnoncourt, M. Muhler, M. Epple, *Eur. J. Inorg. Chem.* **2006**, 4782–4786.
[27] S. Vukojevic, O. Trapp, J. D. Grunwaldt, C. Kiener, F. Schüth, *Angew. Chem.* **2005**, *117*, 8192–8195; *Angew. Chem. Int. Ed.* **2005**, *44*, 7978–7981.
[28] R. Becker, H. Parala, F. Hipler, O. P. Tkachenko, K. V. Klementiev, W. Grünert, H. Wilmer, O. Hinrichsen, M. Muhler, A. Birkner, C. Wöll, S. Schäfer, R. A. Fischer, *Angew. Chem.* **2004**, *116*, 2899–2901; *Angew. Chem. Int. Ed.* **2004** *43*, 2839–2842.
[29] S. Hermes, M. K. Schröter, R. Schmid, L. Khodeir, M. Muhler, A. Tissler, R. W. Fischer, R. A. Fischer, *Angew. Chem.* **2005**, *117*, 6394–6397; *Angew. Chem. Int. Ed.* **2005**, *44*, 6237–6241.
[30] B. Rohe, W. S. Veeman, M. Tausch, *Nanotechnology* **2006**, *17*, 277–282.
[31] G. E. Parris, K. Klier, *J. Catal.* **1986**, *97*, 374–384.
[32] M. Kotecha, B. Rohe, W. S. Veeman, M. Tausch, *Microporous Mesoporous Materials* **2006**, *95*, 66–75.
[33] H. P. Klug, L. E. Alexander, *X-ray diffraction procedures for polycrystalline and amorphous materials*, Wiley-Interscience, New York, **1974**.
[34] D. A. M. Monti, A. Baiker, *J. Catal.* **1983**, *83*, 323–335.
[35] O. Hinrichsen, T. Genger, M. Muhler, *Chem. Eng. Technol.* **2000**, *11*, 956–959.

Received: November 19, 2006
Published Online: March 13, 2007

